Nanoscale

Accepted Manuscript

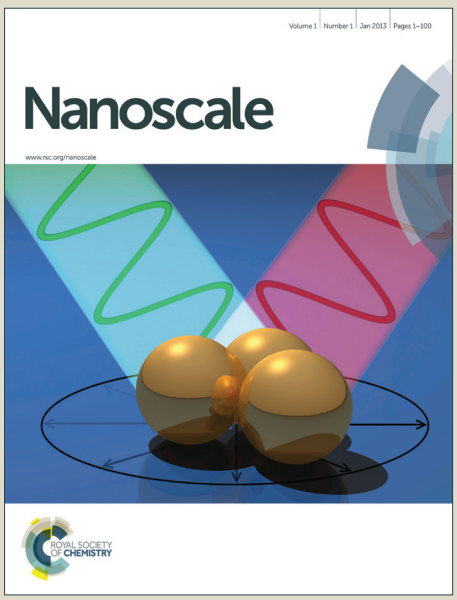

ROYAL SOCIETY OF CHEMISTRY

www.rsc.org/nanoscale

Effects of Nanostructure Geometry on Nanoimprinted Polymer Photovoltaics

Yi Yang,[a] Kamil Mielczarek,[b] Mukti Aryal,[c] Anvar Zakhidov[a,b] and Walter Hu*[a,c]

[a]Department of Materials Science and Engineering, [b]Department of Physics, [c]Department of Electrical Engineering, The University of Texas at Dallas, Richardson, TX 75080, USA

*E-mail: walter.hu@utdallas.edu

Abstract

We demonstrate the effects of nanostructure geometry on the nanoimprint induced poly(3-hexylthiophene-2,5-diyl) (P3HT) chain alignment and the performance of nanoimprinted photovoltaic devices. Out-of-plane and in-plane grazing incident X-ray diffractions are employed to characterize the nanoimprint induced chain alignment in P3HT nanogratings with different *widths, spacings* and *heights*. We observe the dependence of the crystallite orientation on nanostructure geometry such that larger *width* of P3HT nanogratings leads to more edge-on chain alignment while the increase in *height* gives more vertical alignment. Consequently P3HT/[6,6]-penyl-C61-butyric-acid-methyl-ester (PCBM) solar cells with the highest density and aspect ratio P3HT nanostructures show the highest power conversion efficiency among others, which is attributed to the efficient charge separation, transport and light absorption.

Introduction

Conjugated polymers based organic photovoltaics (OPVs) have been subject to increasing research interest over the past years due to the potential of being light weight, mechanically flexible, semitransparent as well as the relatively high power conversion efficiency (PCE) when compared to other types of OPVs such as small molecule solar cells.[1, 2] However, the highest PCE achieved by this type of solar cells is still lower than their inorganic counterparts.[3] To increase their efficiency, one first needs to

achieve a precisely controlled donor/acceptor phase separation within the short exciton diffusion length (~10 nm) without dead ends.[4, 5] Thus far it has been impossible to achieve such a morphology in the most widely used bulk heterojunction (BHJ) structure in which randomly distributed phases cause significant charge recombination.[6] In recent years, nanoimprint lithography (NIL) has been considered to be an effective technique to solve this issue.[7-10] For example, with this technique, an ordered and interdigitized heterojunction can be realized between poly(3-hexylthiophene-2,5-diyl) (P3HT) and [6,6]-penyl-C61-butyric-acid-methyl-ester (PCBM), the most commonly studied donor-acceptor combination.[11-14] The molecular orientation of P3HT can also be controlled by NIL to achieve high hole mobility and solar cell performance. For P3HT solar cells with the active layer vertically sandwiched between anode and cathode as shown in Fig. 1, it is preferable for its molecules to align with an orientation which allows for a smaller hole hopping distance along the vertical electric field direction and a larger hole mobility. Among three typical orientations for P3HT chain alignment, the edge-on is the least favorable due to the large hopping distance *a* (~1.69 nm) along the hexyl side chain which results in a very low hole mobility (~10^{-10} $cm^2/V{\cdot}s$). A large vertical hole mobility (~0.1 $cm^2/V{\cdot}s$) becomes possible if a face-on or vertical orientation can be realized, with the short hopping distances *b* (~0.38 nm) and *c* (~0.38 nm) along the π-π stacking and backbone directions, respectively.[15-20] The actual molecular orientation in the P3HT thin film is a complex mixture of all three kinds of orientations with all kinds of titling angles. Annealing devices at temperatures higher than the T_g of P3HT (~80 ^oC) has been shown to allow the polymer chains to reorder in a more thermodynamically favorable way and increase its crystallinity.[21-23] However it is evident that during annealing, P3HT thin films tend to be aligned with edge-on orientation dominating in the mixture, and thus limit the vertical conductivity.[19, 20, 24, 25] Our previous studies have shown that the portion of vertical orientation in the P3HT film can be significantly enhanced using NIL and it is thus possible to enhance the hole mobility with this technique.[12, 15] The enhancement of vertical alignment by NIL may derive from the interaction between the hydrophobic sidewalls of FDTS coated Si mold and hydrophobic hexyl side chains of P3HT.[24, 26]

Despite the significant progress made in the field, a fundamental understanding of nanostructure geometry effect on the chain alignment of P3HT and OPV performance remains largely unknown. A gap in understanding can be attributed to inconsistent geometries of imprinted P3HT nanostructures used for OPVs, which result in PCEs ranging 0.1-3%.[10, 13, 14, 27-29] It is therefore difficult to compare the results of one work to another. Additionally, all studies in literature investigating NIL induced chain alignment in P3HT have not included solar cell results within the same work to directly prove its impact and demonstrate their correlations.[15, 30, 31] To address these issues here we have systematically studied the effects of nanostructure geometry on both chain alignment and device performance. It is the first time to the best of our knowledge that such a study has been carried out. We first studied the geometry effect on chain orientation by grazing incident X-ray diffraction (GIXRD) measurements of P3HT nanogratings with consistently varied *widths* and *heights*. We found that the crystallite orientation in the imprinted P3HT nanostructures was highly dependent on the nanostructure geometry. A larger *width* of imprinted P3HT nanostructures induced more edge-on alignment due to a larger interaction area with the flat trench bottoms of the Si mold. On the other hand, a larger *height* introduced more vertical alignment because of an increased interaction area with the sidewalls of the mold. Then P3HT/PCBM solar cells with these different feature sizes of P3HT nanogratings were fabricated to study the impacts of nanostructure geometry and chain alignment on the device performance. Consistent with the GIXRD results, the optimal PCE (over 3%) was observed on devices with the narrowest, highest P3HT nanostructures, as well as the largest P3HT/PCBM junction area, which enabled efficient charge separation, transport and light absorption.

Experimental

Fabrication and GIXRD measurement of P3HT nanogratings

In this work, Si nanograting molds with different *heights* and *widths/spacings* were used to control the P3HT nanostructure geometry. All molds were treated with 1*H*,1*H*,2*H*,2*H*-perfluorodecyltrichlorosilane (FDTS) as an anti-adhesion layer. P3HT (Reike Metal, Ltd.) thin films spincoated on Si substrates were

imprinted at 170 °C and 50 MPa for 600 sec. High molecular weight (M_n~30K) P3HT was used in this work because it is not dissolved in dichloromethane (DCM), which serves as an orthogonal solvent to spincoat PCBM when making the solar cell.[7] Also for the XRD experiments, the most commonly used OPV substrate, indium tin oxide (ITO) or poly(3,4-ethylenedioxythiophene):poly(styrenesulfonate) (PEDOT:PSS) coated ITO, was not chosen because the peaks from P3HT and ITO on XRD spectrum are close to each other and affect the result analysis.[32] Si substrate was chosen instead because it exhibits no peaks within the range of interest (5^o-25^o for P3HT). Moreover, people have proven that Si substrate gives the same type of P3HT chain orientation as ITO or PEDOT:PSS coated ITO, and is therefore widely used in literature to simulate the crystallization in solar cells.[15, 30, 32, 33] Fig. 2(a) and (b) show that the nanostructures on a Si mold were transferred into P3HT film with excellent fidelity.

As summarized in Table 1, six different geometries of P3HT structures were made in this work to study the geometry effects on chain alignment and solar cell performance. It should be noted that *residual layer* (*f*) was 20 nm for all imprinted nanostructures. G1, 70 nm flat thin film, was used as reference and its thickness was approximately the same as G2 (*width w*= 280 nm, *spacing p*= 280 nm, *height h*= 110 nm), G3 (*w*= 210 nm, *p*= 210 nm and *h*= 110 nm) and G5 (*w*= 60 nm, *p*= 80 nm and *h*= 110 nm) before they were imprinted into nanostructures. An important factor known as interface enhancement factor (IEF) is used here to characterize the synergistic effects of both *width* and *height* of nanostructures.[10, 34] The IEF describes the ratio of imprinted nanostructure interface area (A) to non-imprinted one (A_0).

$$IEF = A / A_0 = 1 + \frac{2h}{w + p} \quad , \tag{1}$$

As shown in Table 1, *IEF* constantly increased from G1 (1) to G6 (~3.43). In this work we could not increase the *IEF* any further due to our limitations on mold fabrication and de-molding process after NIL. GIXRD measurement was carried out to measure the P3HT chain alignments using a Rigaku Ultima III diffractometer. To find the geometry effects of P3HT nanostructures on different organization directions by NIL, two types of GIXRD setups, *i.e.,* out-of-plane and in-plane, were used to investigate

the chain orientation within the imprinted nanogratings.[15, 35] In both out-of-plane and in-plane measurements, the angular spectrum was collected from 3° to 30° with a wavelength of 0.154 nm and an incident angle $\omega = 0.5^{o}$ with respect to the plane of sample surface. In the out-of-plane GIXRD, the detector is rotated vertically with respect to the sample surface with a scan axis of 2θ, so that the chain alignment along the vertical direction can be studied. While for the in-plane measurement, both sample stage and detector are rotated horizontally with scan axes of ϕ and $2\theta\chi$, respectively, so that the crystallite information along the horizontal directions can be obtained. The detailed out-of-plane and in-plane GIXRD setups are shown in Supporting Information. To characterize the lateral chain orientations perpendicular to and along the nanogratings, the nanograting direction was initially adjusted parallelly and perpendicularly, respectively, to the incident X-ray beam manually with the cross hair labelled on the sample stage. In this work, these two types of measurements were named "parallel to nanogratings" and "perpendicular to nanogratings" because of the nanogratings' initial directions with respect to the incident beams. The irradiation area of X-ray beam in the GIXRD experiments was estimated as 15mm×5mm, smaller than the imprinted samples (20 mm×15 mm).

Solar cell fabrication and characterization

To study the effects of nanostructure geometry on OPV performance, P3HT/PCBM solar cells with different feature sizes of P3HT nanogratings as listed in Table 1 were fabricated in the following structure: ITO/ PEDOT:PSS/P3HT/PCBM/LiF/Al. First a thin layer (~20 nm) of PEDOT:PSS (CLEVIOS P VP Al 4083, H. C. Starck, Inc.) was spin-coated onto the patterned ITO coated glass substrates (Luminescence Technology) and baked at 150 ^{o}C for 15 min. In this work, low conductive PEDOT:PSS was chosen to minimize the measurement error from device areas due to the lateral conductivity of PEDOT:PSS.[34] **Then P3HT thin films were imprinted by a flat mold (Device D1) and molds with different sizes of nanogratings (D2 to D6) to form different geometries under the same conditions as the samples used in GIXRD experiments. After P3HT was processed, an optimized layer of PCBM (Nano-C, Ltd.) with a thickness of 120 nm was spincoated on top from dichloromethane (DCM) as an orthogonal solvent. After spincoating PCBM, no thermal annealing**

was carried out. Thermal annealing was avoided as it would make PCBM and P3HT diffuse into each other, forming a structure similar to the bulk heterojunction, and make it difficult to analyze the effects of nanograting geometry. Finally, 1 nm LiF and 100 nm Al were thermally evaporated on top as the cathode. We did not Four solar cell pixels with an active area of 9 mm^2 each were formed on each substrate. After the OPV devices were made, their current density-voltage (*J-V*) characteristics were measured using Air Mass 1.5 global solar simulated light (AM. 1.5G) calibrated using an NREL traceable KG5 color filtered silicon photodiode (PV Measurements Inc.) to an intensity of 100 mW/cm^2. Open circuit voltage (V_{oc}), short circuit current (J_{sc}), fill factor (FF) and PCE of these devices were extracted from these *J-V* curves. For each kind of devices, the average and standard deviation of device characteristics were calculated from four OPV pixel devices on the same substrate. To further reduce the experimental errors, three batches of P3HT/PCBM solar cells with different sizes of P3HT nanogratings were repeated. Small standard deviations were observed from all devices.

Results and discussion

Effects on chain alignment

In our previous study, we have shown that the portion of vertical orientation in the P3HT film can be significantly enhanced using NIL and it is thus possible to enhance the hole mobility with this technique.[12, 15] The origin of this enhanced vertical alignment by NIL may be from the interaction between the hydrophobic sidewalls of FDTS coated Si mold and hydrophobic hexyl side chains of P3HT.[24, 26] However, it should be noted that since P3HT molecules are interacting with the flat trench bottoms and vertical sidewalls of Si mold at the same time during NIL, it may induce different kinds of chain alignments at the same time because their interaction directions are different. It is reasonable to speculate that the dominant orientation would be determined by the ratio between the area sizes of these two regions, *i.e.* nanostructure geometry. Thus far no work has been reported on it and a good understanding of the correlation between nanostructure geometry and chain alignment has not been established.

To address the issue above, the chain orientation of a series of P3HT nanogratings with various geometries as listed in Table 1 were studied in this work. First of all, three samples were measured by out-of-plane GIXRD, respectively, including $G1_a$ of 70 nm thin film without NIL, $G1_b$ of 70 nm thin film imprinted by a flat Si mold, and G5 of imprinted nanogratings (*w*= 60 nm, *p*= 80 nm and *h*= 110 nm) which was as thick as G1 before imprint. As shown in Fig. 3(a1), (100) peaks at 5.2°, corresponding to lattice parameter *a* and edge-on orientation, were observed for all three samples but with different intensities. $G1_b$ which was imprinted by the flat mold showed a much higher (100) peak than that of $G1_a$ without NIL. However, interestingly, the peak intensity of G5, which was imprinted by nanograting mold, was much lower than that of $G1_a$, It indicates that there were more edge-on orientations when P3HT molecules were interacting with the flat mold horizontally but less when with the nanograting mold vertically. This is because the hydrophobic chains of FDTS on Si mold can favor the interaction with the hydrophobic hexyl side chains of P3HT and make them align with each other, as demonstrated in literature.[24, 26] This chain reordering may start from the interface and propagate into the thin film, due to the side chain to side chain attraction among neighboring P3HT molecules. Flat and nanograting molds can therefore induce different P3HT chain orientations, *i.e.* edge-on alignment dominant for flat mold imprinted samples and face-on or vertical for nanograting mold imprinted samples (due to interactions with vertical sidewalls of the nanograting mold). Since there was no (010) peak in Fig. 3(a) corresponding to lattice parameter *b* at 23.4°, face-on orientations was not detected and it was consistent with our previous study.[15] During imprinting, it is noted that some P3HT molecules were still interacting with the flat trench bottoms of the Si nanograting mold after they fully flowed up. Therefore, the dominant type of chain orientation in P3HT nanogratings would be determined by their geometry, *i.e.*, the ratio between nanograting *width* and *height*. To analyze it, an additional three geometries G3 (*w*= 210 nm, *p*= 210 nm and *h*= 110 nm), G4 (*w*= 60 nm, *p*= 80 nm and *h*= 50 nm) and G6 (*w*= 60 nm, *p*= 80 nm and *h*= 170 nm) were tested and compared with G5 (*w*= 60 nm, *p*= 80 nm and *h*= 110 nm), as shown in Fig. 3(a2). It is found that G3, which had larger nanostructure *width*, the same nanostructure *height* and initial thickness as G5 before imprint, showed a larger (100) peak. This is because of its larger interaction

area with the mold's trench bottoms and smaller area with the sidewalls. In addition, G4 and G6, which had the same *width*/*spacing* as G5 but smaller and larger *heights*, respectively, demonstrated almost the same (100) peak intensity. It means that they had similar amount of edge-on orientations. This is because these three geometries shared the same nanostructure *width*, so that their interaction area with the trench bottoms of the mold was similar. To summarize the findings in Fig. 3(a), one can conclude that the orientation of NIL induced chain alignment is highly dependent on the mold/nanostructure geometry which determines the interaction direction between mold and P3HT polymer chains.

In the out-of-plane GIXRD results above, one can confirm that NIL can change the initial edge-on orientations to some other types by the reduced (100) peak intensity. (010) peak which corresponds to lattice parameter *b* was absent, meaning that face-on orientation was not detected in this study. In-plane GIXRD measurement which reveals the lateral chain orientation is needed to find out if there is any vertical alignment. In this work, G3 to G6 were measured by this technique with gratings parallel and perpendicular to the incident beam initially, as shown in Fig. 3(b1) and 3(b2), respectively. When the X-ray was parallel to the nanograting direction, all nanostructures showed large (100) peaks and ultra-low (010) peaks. However, when nanogratings were perpendicular to the beam, all (100) peaks were quenched and larger (010) peaks were observed. These results demonstrate that the dominant orientation for P3HT crystallites after NIL was vertical alignment, with hexyl side chain spacing *a* perpendicular to and π-π stacking *b* along the grating direction, respectively. Although tiny (010) peaks in Fig. 3(b1) and (100) peaks in Fig. 3(b2) were observed, respectively, indicating that some molecules did not follow this arrangement, the (100) and (010) peak intensities in these two figures were much larger and proved that the configuration above was dominant. It can also be seen that there is a constant increase in both (100) and (010) peak intensities in Fig. 3(b1) and 3(b2), respectively, with the increasing nanograting *height* from G4 to G6, demonstrating that the higher nanostructures contained more vertically aligned polymer chains. It can be explained by the larger interaction area between mold sidewalls and P3HT molecules when larger *height* of mold was used. In addition, compared to all other samples, G3 showed the lowest peaks intensity in both in-plane measurements. This is due to the fact that its interaction area with mold

sidewalls was the smallest and thus induced the smallest amount of vertical alignment. To further clarify the geometry effects on the vertical chain alignment in P3HT, we plotted the integrated intensities (area) of each (100) peaks in Fig. 3(b1) and (010) peaks in Fig. 3(b2) (indication of the density of vertically aligned P3HT crystallites), respectively, for geometries G3-G6 as a function of the factor IEF as defined previously (directly related to the size of mold sidewalls). As shown in Fig. 4(a) and (b), the integrated peak intensity increased almost linearly with IEF. This demonstrates that P3HT nanogratings with larger *height* and density allow for more crystallites with vertical orientation.

Based on the out-of-plane and in-plane GIXRD results, the effects of nanostructure geometry on chain alignment become clearer. More edge-on orientations are present when the nanostructures have a larger *width* but more vertical alignments when they have a larger *height* or IEF. Fig. 5 provides a schematic illustration of molecular alignment in the imprinted P3HT nanogratings with edge-on orientation close to the mold trench bottoms and vertical orientation close to the sidewalls, as suggested by the GIXRD results. From this study one can also speculate that among all geometries in Table 1, G6 is the best for OPVs because of its smallest nanograting *width*, largest *height*, largest IEF, therefore largest amount of vertical chain alignment and possibly highest vertical hole mobility.

In XRD spectra above, the integrated intensity of each peak is proportional to the total population of P3HT crystallites per unit volume. The size of NIL formed P3HT crystallites L can be obtained by the Scherrer formula

$$L \sim \frac{0.9\lambda}{\Delta_{2\theta}\cos(\theta)}\ , \qquad (2)$$

where λ is the X-ray wavelength and $\Delta_{2\theta}$ is the full *width* half maximum of the peak.[18, 19, 36] Applying equation (2) to (100) peaks in Fig. 3(b1) and (010) peaks in Fig. 3(b2) which illustrate the main vertical chain alignment by NIL, one can obtain the crystallite sizes L_a and L_b for G3 to G6 along directions *a* and *b*, respectively. As summarized in Table 2, the crystallite size increased with nanostructure *height* but decreased with nanostructure *width* in both *a* and *b* directions. One possible explanation could be that the

edge-on and vertical alignments are competing with each other during imprint. When the edge-on alignment is dominant, such as in G3, it can affect the vertically aligned crystallite size. More future studies are needed to confirm it. This finding again indicates that G6 would give the highest hole mobility and be the best for solar cells when compared to other geometries in this work.

Effects on solar cell performance

To investigate the impacts of nanostructure geometry and chain alignment on OPV performance, P3HT/PCBM solar cells with different feature sizes of P3HT nanogratings as listed in Table 1 were characterized. The *J-V* characteristics of these devices are shown in Fig. 6. V_{oc}, J_{sc}, FF and PCE of these devices extracted from the *J-V* curves are listed in Table 3. The overall dependences of these results on nanostructure *width*, *height* and IEF are illustrated in Fig. 7. The results have shown that all OPV characteristics J_{sc}, FF and PCE had monotonic increasing correlations with the decreasing *width* and increasing *height* of P3HT nanogratings or with the increasing *IEF* (combined effects of *width* and *height*). Referring to the monotonic increasing correlation of vertical chain alignment (Fig. 4) with *IEF*, the data suggested that the enhancement of device performance would be likely due to the increased heterojunction interface area and enhanced vertical chain alignment in P3HT nanostructures. The effects of these factors on the device performance are further discussed in greater details as follows.

As shown in Fig. 6 and Fig. 7(a), it is found that for D1, D2, D3 and D5 which had the same initial thickness and/or nanograting *height*, the J_{sc} increased constantly with the decrease of nanograting *width*/*spacing*. Since our preliminary study had shown that there were no obvious light absorptance changes for these devices, this impact was firstly ruled out. The first possible explanation is that when the nanostructure size decreased, *i.e.*, closer to the exciton diffusion length, a better charge separation occurred. The second possible reason for this improvement in photocurrent may come from the higher density of vertically aligned crystallites, resulting in increased hole mobility within

the narrower gratings, which has been proven in the previous GIXRD study. Enhanced hole mobility can also result in an increase in FF, which is dependent on the carrier drift length L_d,

$$L_d = \mu \tau E, \quad \textbf{(3)}$$

where μ is the carrier mobility, τ is the carrier lifetime and E is the electric field.[32] Hence a better FF can be expected if there is an increase in mobility within the same active layer thickness, as observed for these devices in Fig. 7(b). D4, D5 and D6 with the same nanostructure *width/spacing*, demonstrated similar and high FFs which can be attributed to their large amount of vertical alignments. It is interesting that the FF in D6 showed the highest value among all devices even though it had the largest *height* (170 nm). It means that the hole mobility and hole drift length in this device must be the highest so that the recombination losses were minimized. We believe this can be explained by its largest crystallite size as shown in Table 2. It is also worth noting that the average FF in D6 was more than 60%, similar to the high values reported for the BHJ structure in literature. Such large improvement on FF suggested that the hole mobility in the P3HT nanogratings was likely improved.[21, 32] It was also in agreement with the monotonically increased vertical chain alignment with *IEF* as shown in Fig. 4. Moreover, D6 showed the highest J_{sc} compared to D4 and D5. In addition to the highest mobility, its largest *height* and thus most efficient light absorption could be a reason as well. As expected from XRD results the performance of D6 with the smallest *width* but largest *height* of P3HT nanostructures was the highest among all six geometries in this study. Other than the impact of *width* and *height*, constant increases in PCE with *IEF* was found as well which highlight the importance of a large donor-acceptor interfacial area, as shown in Fig. 7(c) and 7(d). The average PCE realized in D6 (~3.1%) was three times higher than the non-imprinted D1 (~1.16%) and similar to those typical values (~3-4%) reported in BHJ structure using the same materials.

We believe there is a large room to improve our device performance, as the largest *IEF* of our current devices is only ~ 3.4. To obtain a better PCE, we can further increase the aspect ratio of the

P3HT nanostructures, *i.e.* decrease the *width* and increase the *height*, as predicted by the trend found in this study. The significant enhancement of vertical chain alignment and hole mobility in high aspect ratio nanogratings found in this study would enable the use of high aspect ratio of nanostructures in a thicker active layer. However to achieve this, large area molds with smaller feature sizes need to be made. To enable higher aspect ratio nanostructures, the de-molding process after NIL needs improvement as well. Other possible improvements will include optimizing PCBM thickness according to the new feature size of P3HT nanostructures if achieved and reducing the thickness of P3HT *residual layer* to minimize the light screening. It is worth noting that in this work, the effect of NIL on mobility was studied indirectly and discussed based on the analysis of GIXRD and solar cell results. Other techniques may be utilized if a direct measurement of the vertical hole mobility in P3HT nanostructures is needed.

Conclusions

In this study, the effects of nanostructure geometry on NIL induced P3HT chain alignment and photovoltaic performance are systemically studied. According to the out-of-plane and in-plane GIXRD measurements of P3HT nanogratings with different *widths* and *heights*, the dominant chain orientation by NIL is determined by the Si mold/nanostructure geometry. When the *width* of imprinted P3HT nanostructures is larger, it induces more edge-on alignment due to their larger interaction area with the mold's flat trench bottoms. However, when the *height* is larger, it introduces more vertical alignment because of the larger interaction area with the mold's vertical sidewalls. Imprinted P3HT/PCBM solar cells with the highest PCE are achieved by the narrowest, highest P3HT nanostructures as well as the largest junction area, which is attributed to the efficient charge separation, transport and light absorption.

Acknowledgments

This work is supported by NSF (grant No. ECCS-0901759), Welch Foundation Grant AT-1617, and DOE Phase II STTR program on "Tandem Organic Solar Cells" (grant No. DE-SC00003664). The authors

gratefully acknowledge J. Hsu from Department of Materials Science and Engineering and P. Zang from Department of Electrical Engineering at UT Dallas for their supports and helpful discussions.

References

1. N. S. Lewis, *Science*, 2007, **315**, 798-801.
2. R. F. Service, *Science*, 2011, **332**, 293-293.
3. M. A. Green, K. Emery, Y. Hishikawa, W. Warta and E. D. Dunlop, *Prog. Photovoltaics Res. Appl.* , 2012, **20**, 12-20.
4. J. E. Kroeze, T. J. Savenije, M. J. W. Vermeulen and J. M. Warman, *J. Phys. Chem. B* 2003, **107**, 7696-7705.
5. A. Haugeneder, M. Neges, C. Kallinger, W. Spirkl, U. Lemmer, J. Feldmann, U. Scherf, E. Harth, A. Gugel and K. Mullen, *Phys. Rev. B*, 1999, **59**, 15346-15351.
6. P. K. Watkins, A. B. Walker and G. L. B. Verschoor, *Nano Lett.* , 2005, **5**, 1814-1818.
7. Y. Yang, K. Mielczarek, M. Aryal, A. Zakhidov and W. Hu, *ACS Nano*, 2012, **6**, 2877-2892.
8. S. Y. Chou, P. R. Krauss and P. J. Renstrom, *Science*, 1996, **272**, 85-87.
9. L. J. Guo, *J. Phys. D: Appl. Phys.* , 2004, **37**, R123-R141.
10. Y. Yang, M. Aryal, K. Mielczarek, W. Hu and A. Zakhidov, *J. Vac. Sci. Technol., B* 2010, **28**, C6M104-C106M107.
11. M. Aryal, F. Buyukserin, K. Mielczarek, X. Zhao, J. Gao, A. Zakhidov and W. Hu, *J. Vac. Sci. Technol., B* 2008, **26**, 2562-2566.
12. M. Zhou, M. Aryal, K. Mielczarek, A. Zakhidov and W. Hu, *J. Vac. Sci. Technol., B* 2010, **28**, C6M63-C66M67.
13. X. He, F. Gao, G. Tu, D. G. Hasko, S. Huettner, N. C. Greenham, U. Steiner, R. H. Friend and W. T. S. Huck, *Adv. Funct. Mater.* , 2011, **21**, 139-146.
14. W. Wiedemann, L. Sims, A. Abdellah, A. Exner, R. Meier, K. P. Musselman, J. L. MacManus-Driscoll, P. Mueller-Buschbaum, G. Scarpa, P. Lugli and L. Schmidt-Mende, *Appl. Phys. Lett.* , 2010, **96**, 263109.
15. M. Aryal, K. Trivedi and W. Hu, *ACS Nano*, 2009, **3**, 3085-3090.
16. H. Sirringhaus, P. J. Brown, R. H. Friend, M. M. Nielsen, K. Bechgaard, B. M. W. Langeveld-Voss, A. J. H. Spiering, R. A. J. Janssen, E. W. Meijer, P. Herwig and D. M. de Leeuw, *Nature*, 1999, **401**, 685-688.
17. T. A. Chen, X. M. Wu and R. D. Rieke, *J. Am. Chem. Soc.* , 1995, **117**, 233-244.
18. U. Zhokhavets, T. Erb, H. Hoppe, G. Gobsch and N. S. Sariciftci, *Thin Solid Films* 2006, **496**, 679-682.
19. T. Erb, U. Zhokhavets, G. Gobsch, S. Raleva, B. Stuhn, P. Schilinsky, C. Waldauf and C. J. Brabec, *Adv. Funct. Mater.* , 2005, **15**, 1193-1196.
20. H. Sirringhaus, R. J. Wilson, R. H. Friend, M. Inbasekaran, W. Wu, E. P. Woo, M. Grell and D. D. C. Bradley, *Appl. Phys. Lett.* , 2000, **77**, 406-408.
21. G. Li, V. Shrotriya, J. S. Huang, Y. Yao, T. Moriarty, K. Emery and Y. Yang, *Nat. Mater.* , 2005, **4**, 864-868.
22. T. J. Prosa, M. J. Winokur, J. Moulton, P. Smith and A. J. Heeger, *Macromolecules*, 1992, **25**, 4364-4372.
23. Y. Kim, S. A. Choulis, J. Nelson, D. D. C. Bradley, S. Cook and J. R. Durrant, *Appl. Phys. Lett.* , 2005, **86**, 063502.
24. R. J. Kline, M. D. McGehee and M. F. Toney, *Nat. Mater.* , 2006, **5**, 222-228.
25. M. Brinkmann and J. C. Wittmann, *Adv. Mater.* , 2006, **18**, 860-863.
26. K. Yamamoto, S. Ochiai, X. Wang, Y. Uchida, K. Kojima, A. Ohashi and T. Mizutani, *Thin Solid Films* 2008, **516**, 2695-2699.

27. D. Cheyns, K. Vasseur, C. Rolin, J. Genoe, J. Poortmans and P. Heremans, *Nanotechnol.*, 2008, **19**, 424016
28. X. He, F. Gao, G. Tu, D. Hasko, S. Huettner, U. Steiner, N. C. Greenham, R. H. Friend and W. T. S. Huck, *Nano Lett.* , 2010, **10**, 1302-1307.
29. W. Zeng, K. S. L. Chong, H. Y. Low, E. L. Williams, T. L. Tam and A. Sellinger, *Thin Solid Films* 2009, **517**, 6833-6836.
30. H. Hlaing, X. Lu, T. Hofmann, K. G. Yager, C. T. Black and B. M. Ocko, *ACS Nano*, 2011, **5**, 7532-7538.
31. D. E. Johnston, K. G. Yager, H. Hlaing, X. Lu, B. M. Ocko and C. T. Black, *ACS Nano*, 2013, **8**, 243-249.
32. W. L. Ma, C. Y. Yang, X. Gong, K. Lee and A. J. Heeger, *Adv. Funct. Mater.* , 2005, **15**, 1617-1622.
33. D. Chen, W. Zhao and T. P. Russell, *ACS Nano*, 2012, **6**, 1479-1485.
34. Y. Yang, K. Lee, K. Mielczarek, W. Hu and A. Zakhidov, *Nanotechnol.*, 2011, **22**, 485301.
35. J.-F. Chang, B. Sun, D. W. Breiby, M. M. Nielsen, T. I. Sölling, M. Giles, I. McCulloch and H. Sirringhaus, *Chem. Mater.* , 2004, **16**, 4772-4776.
36. A. L. Patterson, *Phys. Rev.*, 1939, **56**, 978-982.

Table 1 Summary of P3HT structures with different geometries.

Geometry (G) No.	G1	G2	G3	G4	G5	G6
width/*spacing* (nm)	-	280/280	210/210	60/80	60/80	60/80
height (nm)	70 (thin film)	110	110	50	110	170
residual layer (nm)	-	20	20	20	20	20
IEF (A/A_0)	1	1.39	1.52	1.71	2.57	3.43

Table 2 Summary of geometry effect on the sizes of P3HT crystallites formed by nanoimprint.

Geometry (G) No.	G3	G4	G5	G6
width/*spacing*/*height* (nm)	210/210/110	60/80/50	60/80/110	60/80/170
L_a (nm)	12.82	13.71	13.95	15.59
L_b (nm)	6.39	7.11	7.06	7.88

Table 3 Performance of P3HT/PCBM photovoltaic devices built on P3HT nanogratings with different geometries.

Device	D1	D2	D3	D4	D5	D6
width/*spacing*/*height* (nm)	70 nm thin film	280/280/110	210/210/110	60/80/50	60/80/110	60/80/170
IEF = A/A_0	1	1.39	1.52	1.71	2.57	3.43
V_{oc} (V)	0.53±0.01	0.54±0.01	0.53±0.01	0.56±0.01	0.55±0.01	0.57±0.00
J_{sc} (mA/cm^2)	5.47±0.67	6.42±0.06	6.48±0.09	7.42±0.42	8.23±0.19	9.16±0.30
FF	0.40±0.02	0.47±0.01	0.50±0.01	0.58±0.02	0.60±0.01	0.61±0.01
PCE (%)	1.16±0.14	1.61±0.02	1.72±0.05	2.40±0.10	2.67±0.08	3.16±0.07

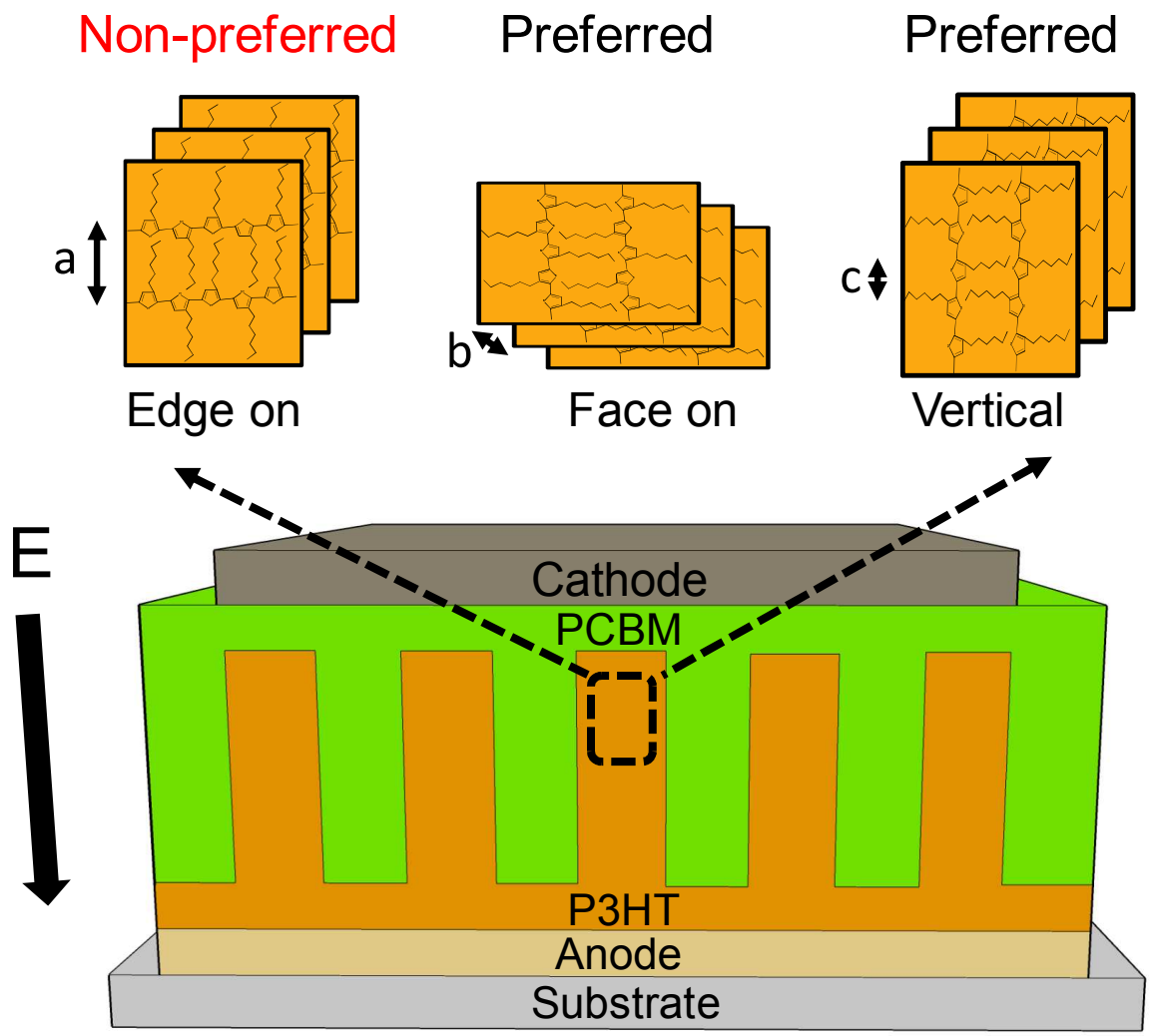

Fig. 1 Schematic of edge-on, face-on and vertical chain orientations of P3HT molecules in a nanoimprinted OPV device of vertically interdigitized and bi-continuous P3HT and PCBM heterojunction. Face-on and vertical orientations are preferred for hole transport due to theirs short hopping distances *b* and *c*, respectively, along the vertical direction of electric field E, compared to the non-preferred edge-on with a large hopping distance *a*.

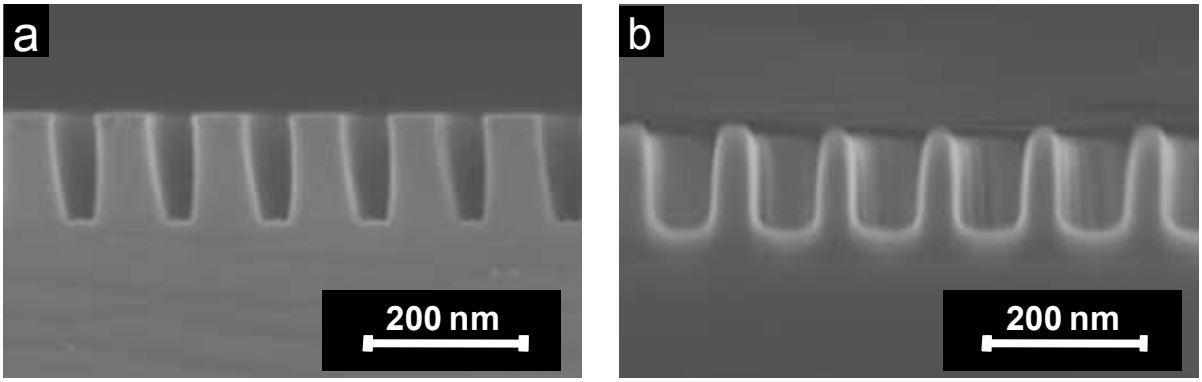

Fig. 2 SEM images of (a) Si nanograting mold and (b) imprinted P3HT nanostructures with *height h*= 170 nm, *width w*= 60 nm and *spacing p*= 80 nm.

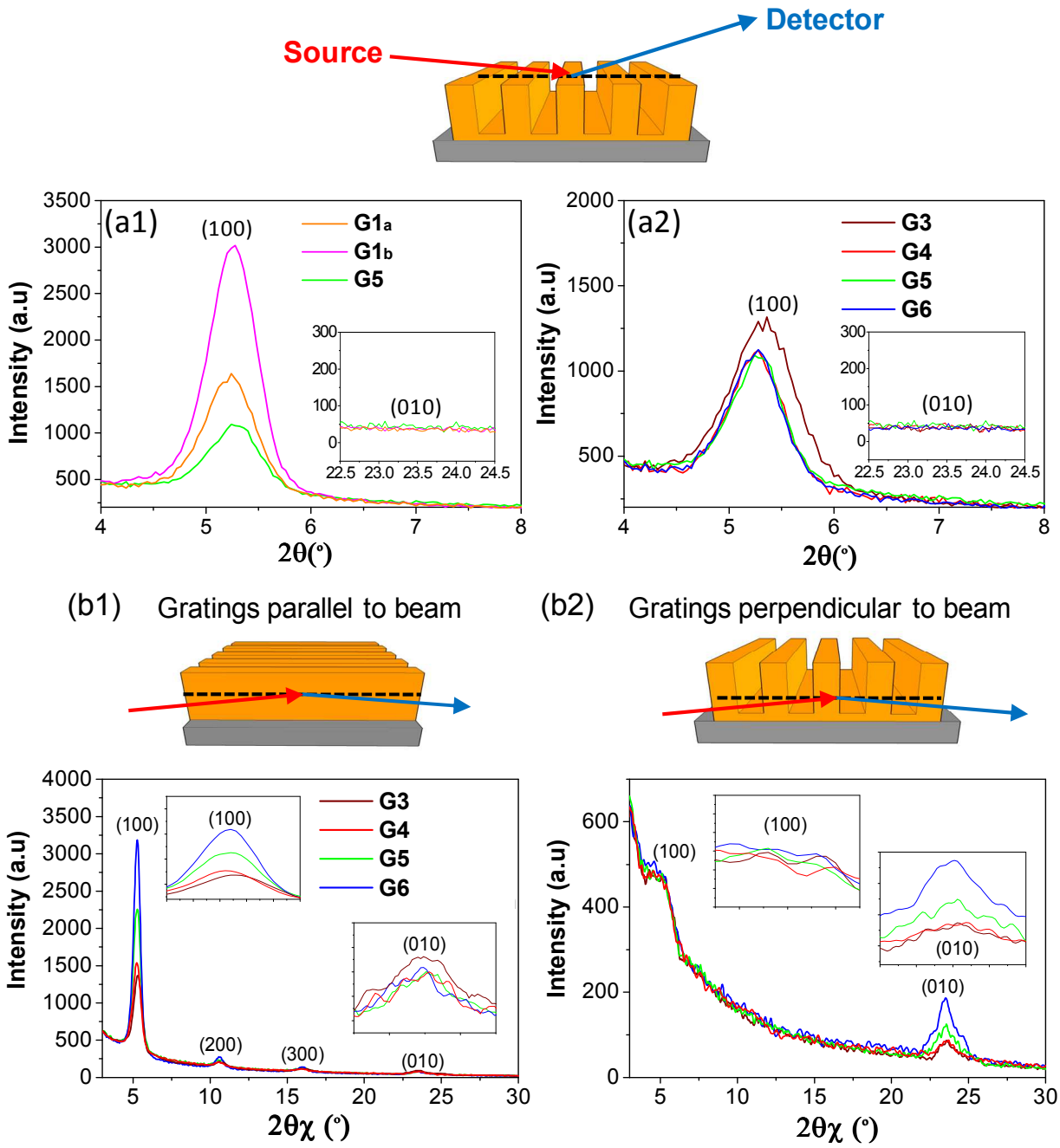

Fig. 3 (a) Out-of-plane GIXRD measurements of P3HT chain orientations with different P3HT geometries: (a1) 70 thin film ($G1_a$) as coated, 70 thin film ($G1_b$) imprinted by a flat mold and nanogratings with *width* w=60 nm and *height* h=110 nm (G5), respectively; (a2) nanogratings with w=210 nm and h=110 nm (G3), w=60 nm and h=50 nm (G4), w=60 nm and h=110 nm (G5), w=60 nm and h=170 nm (G6), respectively. (b) In-plane GIXRD measurements with imprinted nanograting direction (b1) parallel and (b2) perpendicular to the incident X-ray beam initially. The inset figures in (a1) and (a2) show the views of the (010) peaks. The inset figures in (b1) and (b2) show the magnified views of the (100) peaks and (010) peaks, respectively. The same normalization constant is used for all four figures.

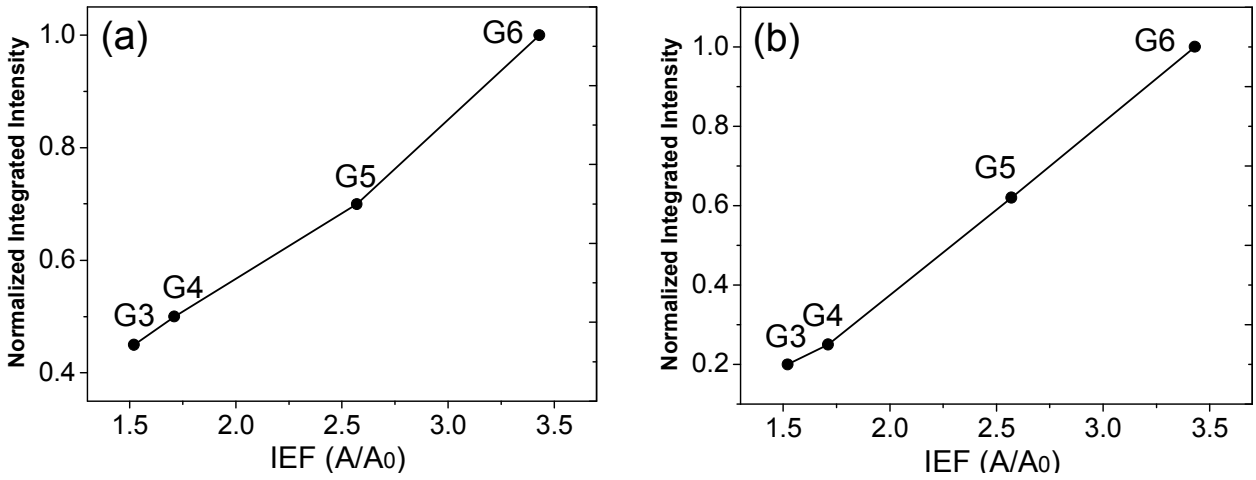

Fig. 4 The effects of IEF (A/A_0) on the normalized integrated intensities (peak area) of (a) (100) peaks in Fig. 3(b1) and (b) (010) peaks in Fig. 3(b2), which are proportional to the total numbers of P3HT crystallites with vertical orientation per unit volume for geometry G3, G4, G5 and G6.

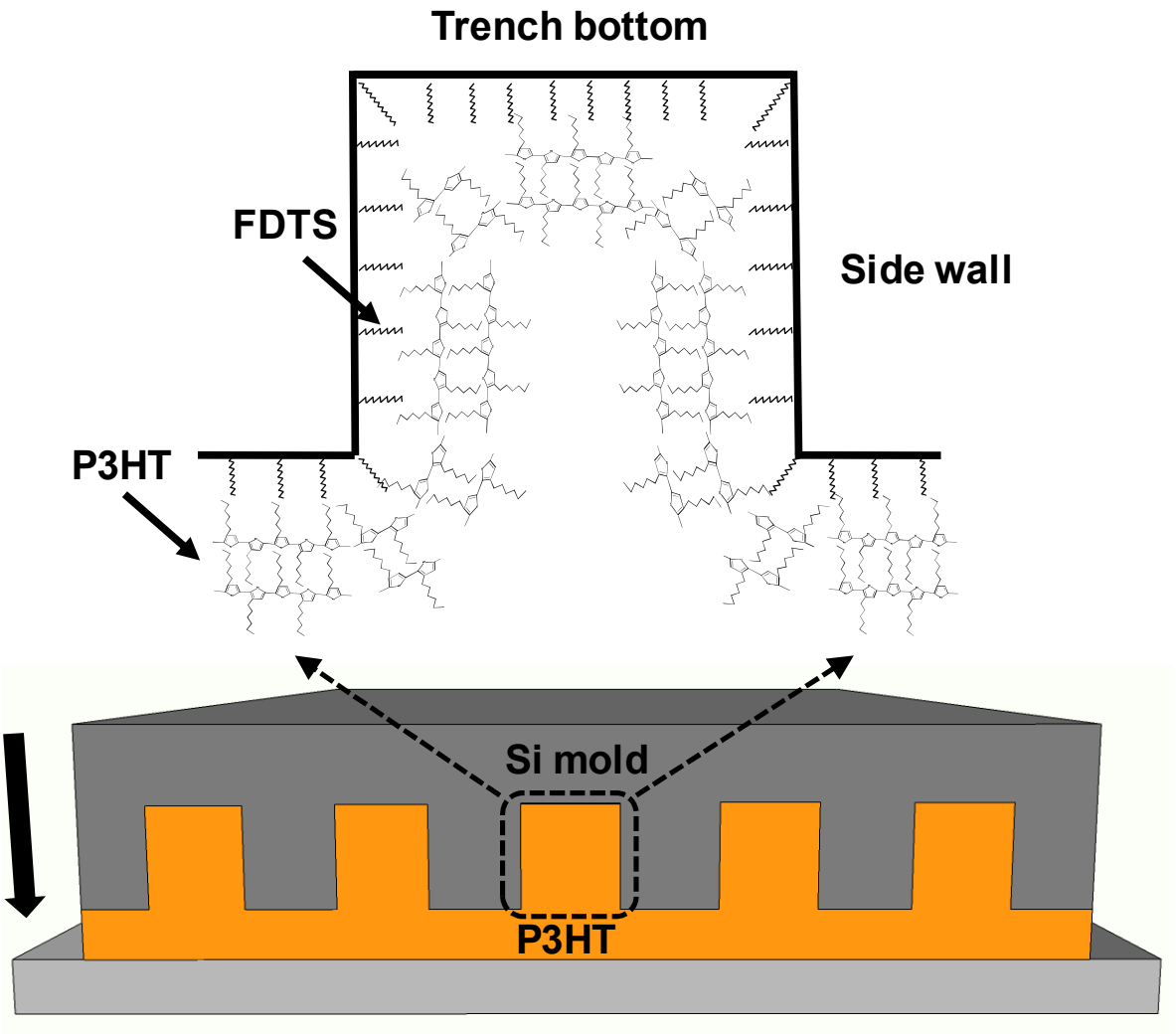

Fig. 5 Schematic of imprinted P3HT nanostructures with edge-on orientation close to the mold trench bottoms and vertical orientation close to mold sidewalls.

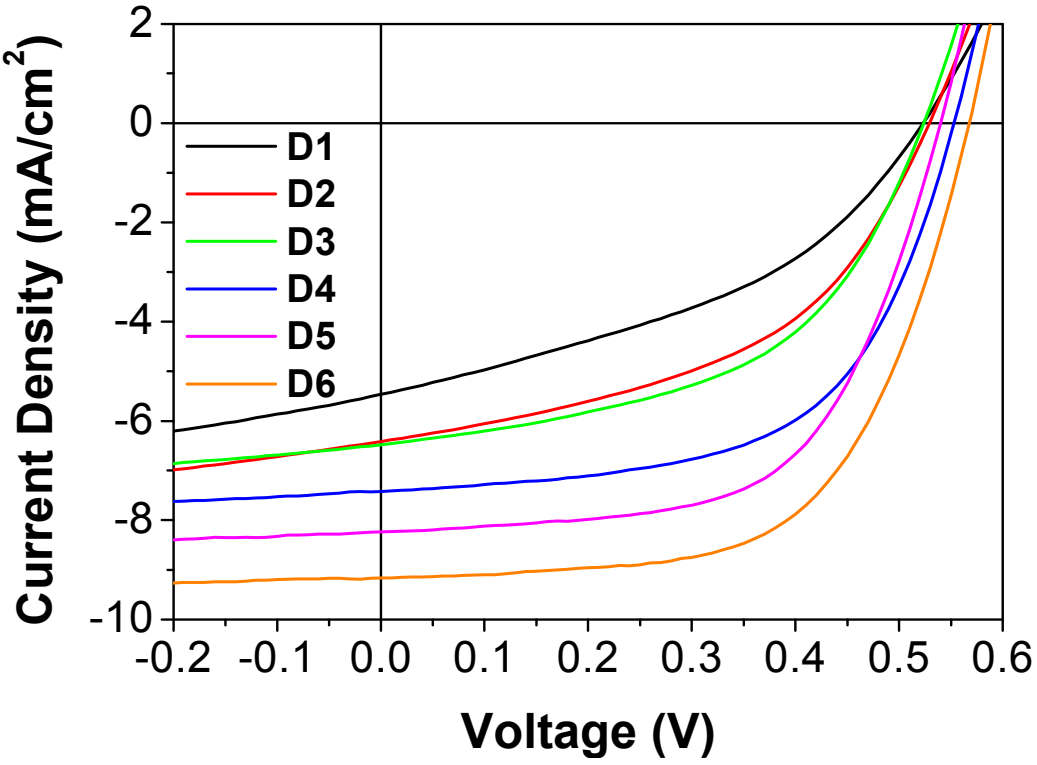

Fig. 6 *J-V* characteristics of P3HT/PCBM solar cells built with different P3HT geometries: non-imprinted 70 thin film (D1), nanogratings with *width*/*spacing* and *height* of 280 nm and 110 nm (D2), 210 nm and 110 nm (D3), 60 nm and 50 nm (D4), 60 nm and 110 nm (D5) and 60 nm and 170 nm (D6), respectively.

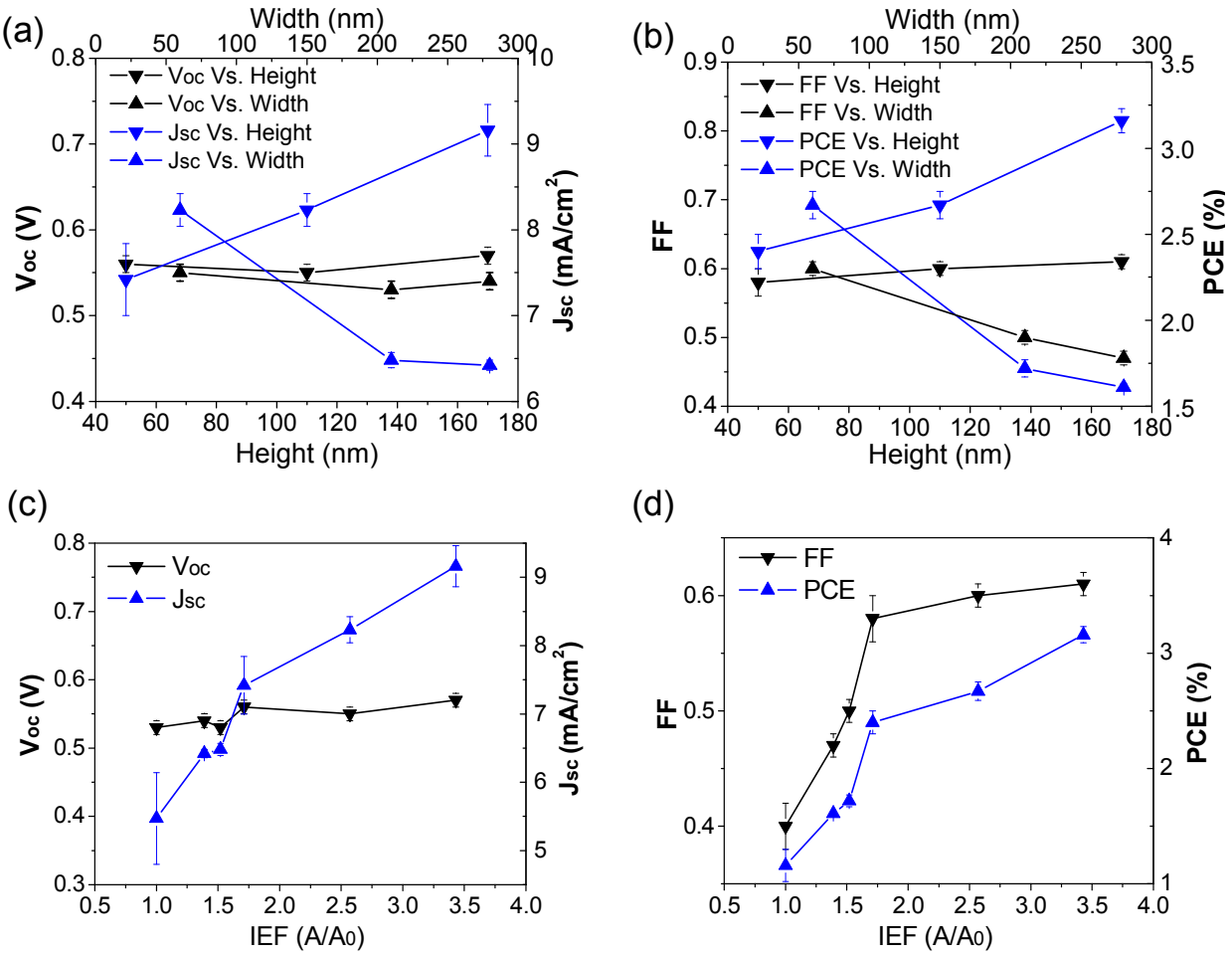

Fig. 7 The impacts of P3HT nanograting geometry on imprinted P3HT/PCBM solar cell performance: (a,b) the *width*/*height* and (c,d) IEF (A/A_0) effects on V_{oc}, J_{sc}, FF and PCE, respectively.